Electrical Power and Energy Systems 101 (2018) 116–126

Contents lists available at ScienceDirect

Electrical Power and Energy Systems

journal homepage: www.elsevier.com/locate/ijepes

Performance analysis and evaluation of reactive power compensating electric spring with linear loads

Jayantika Soni*, Binita Sen, V.K. Kanakesh, S.K. Panda

Department of Electrical and Computer Engineering, National University of Singapore, 4 Engineering Drive 3, Singapore 117583, Singapore

ARTICLE INFO

Keywords:
Inverter
Microgrid
Renewable energy
Smartgrid
VAR compensator

ABSTRACT

Reliance on renewable energy sources (RESs) such as solar and wind has increased to build a sustainable environment, however, their substantial implementation is hindered by their intermittency. Electric Spring (ES) is one of the technologies to mitigate the intermittent nature of the RESs. In an isolated RES powered microgrid, the ES in conjunction with the non-critical loads in a system like water heaters, refrigerators, and air-conditioners can regulate voltage of critical loads like security system, servers etc. This paper establishes the operating principles of the ES (with reactive power compensation only) and its interaction with RESs based on the understanding of AC power transfer between two sources. The accurate phasors in a system under two scenarios, with and without ES, are drawn. Also, performance of the ES is analyzed and evaluated with respect to variations in the loads (linear) and their types. It is augmented with analytical justifications and validated through simulations and experimental studies. Also, through analytical expressions, simulations, and experiments the importance of the non-critical load on the performance of the ES is illustrated. It is also highlighted that the compensation capabilities of the ES remain the same irrespective of the types of non-critical load.

1. Introduction

There has been an increased interest in microgrids powered with renewable energy sources (RESs) like solar and wind in countries all across the world including Singapore [1–3]. An increased penetration of intermittent power from RESs could cause destabilization of the microgrid [4]. A more reformed way of thinking to utilize this intermittency to an economical advantage to the consumer is required. Unlike a traditional grid where demand is non-interactive, the demand of the microgrid is interactive with the grid and can provide cost-effective reliability, balancing, and load-shaping support for the grid [5].

The concept of Electric Spring (ES) was introduced in [6,7] which utilized a power electronic converter to implement demand side management (DSM) and mitigate intermittency of RESs powered grids. The ES is employed in series with the building's non-critical (NC) loads like air-conditioners, refrigerators, water heaters etc. This series combination of the ES and the NC load is called a *smart load* which in turn is attached in parallel to building's critical loads like security system, servers etc. A system configuration is depicted in Fig. 1, where the ES is implemented using an inverter. Initially, in [7,6] the ES is introduced as a reactive power compensator which provided voltage and power stability to a constant impedance load. The capability of the ES to provide a combination of reactive power and real power injection and absorption is highlighted in [8]. Validation of the ES, proof-of-concept hardware, and proof that it could provide load power shedding for the NC load are presented in [9]. Insights on how buildings, an essential part of future microgrids, could serve as grounds for implementation of the ES are outlined in [10]. Analytical reasoning on how storage requirements would be reduced in a system with the ES is given in [11]. Various methods on how the ES could be used to implement power factor correction along with voltage stability in the system are discussed in [12–15]; this version of the ES utilized both real and reactive power compensation from a battery based ES. The dynamic model of the ES is presented in [16] and small-signal model and stability of multiple ESs is discussed in [17]. Frequency regulation using the ES is discussed in [18,19]. Other configurations of the ES have also been developed such as back-to-back ES [20] and DC ES [21–23].

This paper investigates into the operating principles and performance of the ES with only reactive power compensation capabilities, as the present literature has left significant gaps and lacks a deeper analysis. Most of the literature mention that the ES injects capacitive or inductive power in order to boost or reduce the critical load voltage [6,9,8,24,10,25]. The capability of real and/or reactive power compensation by the ES (with an active power source) is highlighted in [8], the authors have suggested that the behavior of such an ES should be according to the type of the noncritical load. However, such a statement

* Corresponding author.
E-mail address: jayantika.soni@u.nus.edu (J. Soni).

https://doi.org/10.1016/j.ijepes.2018.03.017
Received 23 October 2017; Received in revised form 21 January 2018; Accepted 11 March 2018

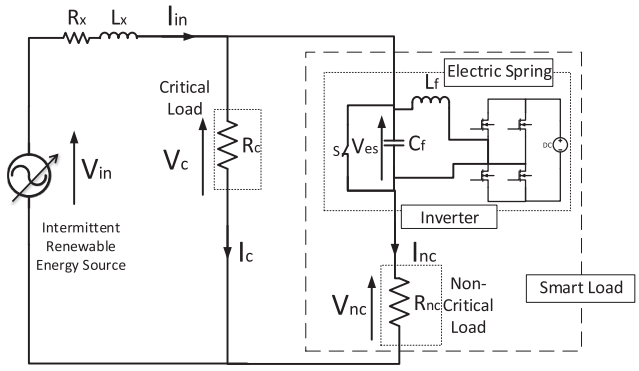

Fig. 1. Circuit diagram of an electrical power system with the electric spring.

cannot be extended for the ES with only reactive power compensation capabilities as considered in this chapter. It is asserted that for voltage regulation, using only reactive power compensation capability of the ES, the behavior of the ES shouldn't change with the type of the non-critical load. The phasor diagrams reflecting this are drawn. The performance of the ES is evaluated by changing the type of critical and the noncritical loads through extensive simulation and hardware experiments. A system with inductive line impedance has been considered and our simulations and hardware experiments prove that the ES injects reactive power to boost voltage in undervoltage conditions and absorbs reactive power to reduce voltage in overvoltage conditions. This is substantiated by valid theory and taking into account the interactions between the two AC power sources in the system, the RES and the ES, connected by an inductive line impedance. Such a theory hasn't been covered in any of the available literature yet to the best of authors' knowledge. To better understand the effects of adding the ES, phasor diagrams of the system both with and without the ES are drawn. Additionally, phasor diagrams according to the behavior of the ES with various non-critical load types are presented in this paper. The literature [16] claims that the performance of the ES is dependent on the ratio of critical and noncritical (NC) load impedances. However, in the pursuit of this research it is revealed ratio might not be enough to judge the performance of the ES. It is found that the performance of the ES relies on the wholesome contribution of the absolute value of the noncritical load impedance. Also, the performance of the ES is evaluated on variation of the impedances and types of critical and non-critical loads through extensive simulation and hardware experiments.

In Section 2 of this paper, parallels from the AC power transmission system are drawn to study the interaction between the RES and the ES. Based on the theoretical knowledge, the behavior of the ES for voltage regulation, in undervoltage and overvoltage scenarios is formulated. Building on this understanding, the system phasor diagrams before and after implementation of the ES are drawn and explained in detail. Further, the impact of changes in system parameters like critical and non-critical impedances and their types and limitations of the ES are studied in Section 2 and validated through simulations and experiments in Section 3. Finally, conclusions from the analysis of operation and performance of ES are drawn in Section 5 and some remarks are made in Section 4.

2. Operating principles of electric spring

Before delving into the operating principles of the ES, it is necessary to grasp what happens when there are two active energy sources in a system. For simplification, a system like in Fig. 2 is studied with two energy sources labeled as G_S (RES) at sending end and G_R (ES) at the receiving end connected through a inductor of impedance, X [26]. The complex power at the receiving end (source G_R), S_R is given by (1) [26], where V_R and V_S are the voltages of sources G_R and G_S, respectively, I is the current flowing through line impedance, and δ is the power angle.

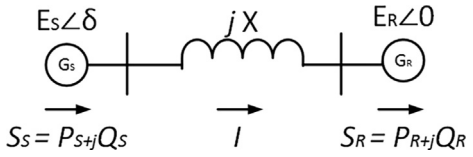

Fig. 2. Power transfer between two power sources.

$$\overrightarrow{S_R} = \overrightarrow{E_R I}^{*} = E_R\left[\frac{E_S\cos\delta + jE_S\sin\delta - E_R}{jX}\right]^{*} \tag{1}$$

In the case where there is no real power transfer between them, the power angle (δ) is zero and the system equations for real power (P_R) of source G_R and real power (P_S) of source G_S are given by (2) and for reactive power (Q_R) of source G_R and reactive power (Q_S) of source G_S are given by (3) and (4), respectively.

$$P_R = P_S = 0 \tag{2}$$

$$Q_R = \frac{E_R(E_S - E_R)}{X} \tag{3}$$

$$Q_S = \frac{E_S(E_S - E_R)}{X} \tag{4}$$

In (3) and (4) when $E_S > E_R$,Q_S and Q_R are positive, that means reactive power is transferred from source G_S to source G_R. This means that when lagging current flows through the inductive line impedance, receiving end voltage (E_R) is lower than the sending end voltage (E_S)). Conversely, when $E_S < E_R$,Q_S and Q_R are negative, that means reactive power is transferred from source G_R to source G_S. This implies when a capacitive current flows through the inductive line impedance, receiving end voltage (E_R) is more than the sending end voltage (E_R) [26].

This understanding from AC power transmission systems is applied to the system where the ES is deployed. In our problem statement, the isolated microgrid system consists of two energy sources namely the RES and the ES (Fig. 1) and power transfer between them would change the behavior of voltage at receiving end that is, critical load voltage, V_c. The ES doesn't exchange any real power with the RES. So, when a lagging current flows through the line inductance, critical load voltage would be reduced and when a leading current flows, critical load voltage would be boosted. For example, consider a system with only resistive critical and non-critical loads and the ES injects only reactive power. In this system, there are following two scenarios to be considered:

- *Undervoltage Scenario*: When the critical load voltage, V_c is less than its reference voltage, V_{ref}, the ES should inject reactive power to boost the critical load voltage. In other words, the ES should behave as a capacitor, so as to make the current through line inductance capacitive. The phasor diagrams of the system, before and after implementation of the ES are shown in Fig. 3a and b, respectively.
- *Overvoltage Scenario*: When the critical load voltage, V_c is more than its reference voltage, V_{ref}, the ES should absorb reactive power to reduce the critical load voltage. In other words, the ES should behave as an inductor, so as to make the current through line inductance inductive. The phasor diagrams for the system, before and after implementation of the ES are shown in Fig. 4a and b, respectively.

In Figs. 3a, b, 4a, and b, V_{in},V_c,V_{nc}, and V_{es} are the input voltage, critical load voltage, non-critical load voltage, and ES voltage, respectively and I_{in},I_c, and I_{nc} are the currents through line impedance, critical load, and non-critical load, respectively. The line resistance and reactance are designated by R_x and X_x, respectively. The system equations for the ES, as shown in Fig. 1, are given by (5)–(7) where, θ_c,θ_{nc} and θ_{es} are the phase angles of the critical load voltage, the non-critical load voltage, and the ES voltage, respectively, ϕ_{nc} is the phase angle of the

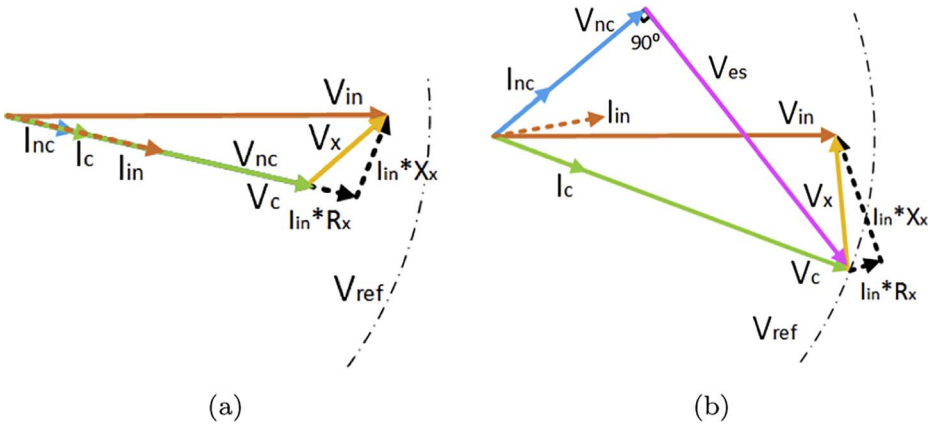

Fig. 3. Phasors of electrical signal in a system in undervoltage scenario ($V_c < V_{ref}$) (a) without ES, (b) with ES.

non-critical load current, Z_{nc} is the impedance of the non-critical load, R_{nc} is the resistance of the non-critical load, and X_{nc} is the reactance of the non-critical load.

$$\vec{V_c} = \vec{V_{es}} + \vec{V_{nc}} \tag{5}$$

$$\vec{I_{nc}} = \frac{\vec{V_{nc}}}{Z_{nc}} = \frac{\vec{V_c} - \vec{V_{es}}}{Z_{nc}} \tag{6}$$

$$I_{nc} = \left[\frac{V_c^2 + V_{es}^2 - 2V_c V_{es}\cos(\theta_c - \theta_{es})}{R_{nc}^2 + X_{nc}^2}\right]^{1/2} \tag{7}$$

The ES is controlled to provide only reactive power compensation using the control scheme as depicted in Fig. 5. It is ensured that V_{es} is orthogonal to I_{nc}. The root mean square (RMS) value of V_c is V_{ref} of 110 V. The error between V_c and V_{ref} is fed to a proportional integral (PI) controller. The output of PI controller is indicative of the magnitude of the ES voltage, V_{es}. The phase angle of the ES voltage is determined by orthogonally shifting the signal generated by the combination of the phase locked loop (PLL) signal with V_{nc} and the power factor angle of the non-critical load, ϕ as shown in Fig. 5. It is to be noted that ϕ would be positive for resistive-inductive or inductive loads and negative for resistive-capacitive or capacitive loads.

2.1. Behaviour of the ES with loads

The ES injects reactive power to boost the critical load voltage (V_c) and absorbs reactive power to reduce the critical load voltage. It is asserted that the ES should behave in the same manner irrespective of the type of non-critical load.

Consider a system with an R-L non-critical load and a resistive critical load. Thus, the input current (I_{in}) of the system without the ES in both undervoltage and overvoltage scenarios would be inductive. In the undervoltage scenario, the ES acts as a capacitor and makes I_{in} capacitive and boosts the critical load voltage, V_c to the reference value (V_{ref}) as shown in Fig. 6a. Conversely, in the overvoltage scenario I_{nc} is not inductive enough to regulate the critical load voltage to reference value. The ES acts as an inductor and makes I_{in} further inductive so as to regulate V_c to V_{ref} as shown in Fig. 6b. Similarly, in a system with a R-C non-critical load the ES would show identical behavior. The ES would act as a capacitor in the undervoltage scenario as shown in Fig. 7a to regulate V_c. In the overvoltage scenario, the ES would act as an inductor as shown in Fig. 7b to regulate V_c.

2.2. Impact of load impedance variation

The ES is controlled to provide only reactive power compensation using the control scheme (Fig. 5). The reactive power compensation by the ES (Q_{es}) should be limited so as to maintain stability in the system, as sudden change in the reactive power supply or demand could lead to voltage instability in the microgrid system [27]. Thus, a physical limit exists for how much reactive power compensation could be obtained from the ES while maintaining voltage stability in the microgrid which has substantially less inertia than the traditional grid.

$$Q_{es} = V_{es}\cdot I_{nc}\cdot\sin(90°) = V_{es}\cdot\left[\frac{V_c^2 + V_{es}^2 - 2V_c V_{es}\cos(\theta_c - \theta_{es})}{Z_{nc}^2}\right]^{1/2} \tag{8}$$

To determine the critical load voltage regulation range, the system Eqs. (5)–(7) are mathematically analyzed and solved with constraint of only reactive power injection by the ES. The system variables are converted into single phase *d-q* axes and it is ensured that the ES Voltage has no *d*-axis component (so that ES provides only reactive power compensation). By iteratively varying the critical load voltage value, the value of reactive compensation required by the ES to maintain critical load voltage to reference value is calculated. It is observed that the solution only exists for a certain range of the critical load voltage compensation for different load conditions and beyond which no solution can be obtained. Thus, the ES would be able to boost or reduce the critical load voltage in a certain range called the compensation range of the critical load voltage. This compensation range is dependent on the ES's reactive power, Q_{es}.

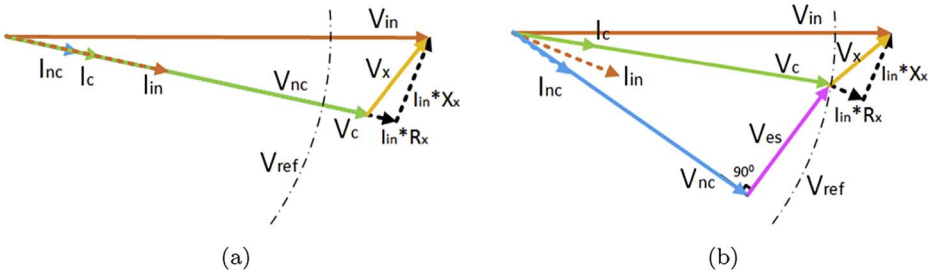

Fig. 4. Phasors of electrical signal in the system in overvoltage scenario ($V_c > V_{ref}$) (a) without ES, (b) with ES.

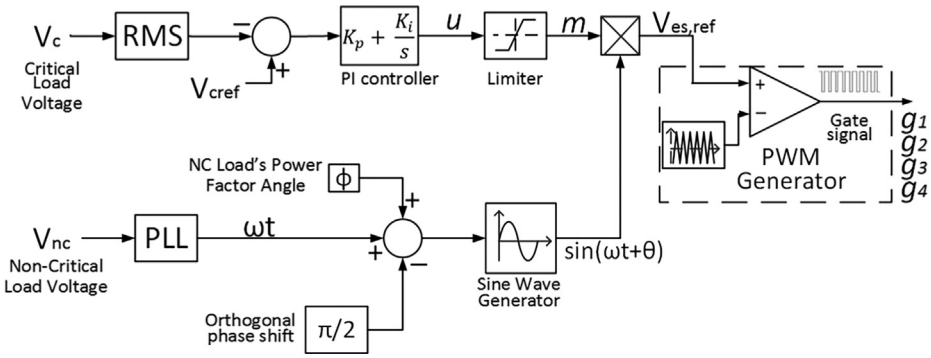

Fig. 5. Control block diagram of ES.

From (8) it can be seen that Q_{es} is dependent on the current through the non-critical load, I_{nc} which is in turn inversely proportional to the impedance of non-critical load, Z_{nc}. Thus, as the impedance of non-critical load decreases, the reactive power injected by the ES would increase and thus the compensation range of the critical load voltage will increase. Moreover, as it could be seen from (8), the reactive power injection is governed by the absolute impedance of the non-critical load, Z_{nc}, the magnitude of the ES voltage, V_{es}, the phase angle of the critical load voltage, θ_c, and the phase angle of the ES voltage, θ_{es}. The magnitude of the critical load voltage, V_c is constant, maintained at its reference value (V_{ref}) of 110 V. Since Q_{es} is not dependent on impedance of the critical load, Z_c in anyway, the ratio of critical and non-critical load impedances shouldn't play a role in the performance of the ES.

2.3. Impact of the type of load

The ES is controlled in such a manner that it provides only reactive power compensation in the system and provides voltage stability using the control scheme illustrated in Fig. 5. However, since it operates in the RES powered microgrid it has its limitations. The microgrid is more susceptible to instability with sudden change in reactive power, thus reactive power demand or supply must be controlled properly to avoid converter reactive limit or system oscillation [27].

To understand the behavior of the ES with resistive-reactive non-critical loads, let's first take the case with a resistive-inductive non-critical load and a resistive critical load and ignore the small reactive power consumed by line impedance. In the undervoltage scenario, the ES injects reactive power, so the overall reactive power of the system will be the net sum of ES's capacitive power and inductive power of the NC load. Thus, the ES could inject more reactive power without affecting system's stability and increases the boosting compensation range of the critical load voltage. Further, in the overvoltage scenario, the ES absorbs reactive power and the NC load too has an inductive power component, thus the reduction compensation range of the critical load voltage would be decreased so as to maintain the stability in the system.

Conversely, with a resistive-capacitive NC load, the ES would absorb more reactive power in the overvoltage scenario and increases the reduction compensation range. In the undervoltage scenario, the ES would inject less reactive power and reduces the boosting compensation range to maintain voltage stability in the system. This has been analyzed mathematically using MATLAB solvers and through simulations and it is observed that the compensation range changes with the type of the NC load with the same impedance, Z_{nc}. The ES's ability to compensate the critical load voltage depends on the non-critical load's absolute impedance value and its type. It is quintessential to gauge performance of the ES in simulation and hardware. The behavior of the ES in such conditions would give more insights into designing control schemes so as to utilize the true potential of the device.

In a nutshell, the reactive power compensating ES injects reactive power to boost the critical load voltage and absorbs reactive power to reduce the critical load voltage, irrespective of the load type. The performance of the ES is not affected by the critical load impedance and its type. However, the type and the impedance of the non-critical load affect the performance of the ES significantly. The compensation range provided by the ES increases with decrease in noncritical load impedance.

3. Validation and performance analysis of the electric spring

To thoroughly test and validate the analysis developed in Section 2, the ES has been subjected to diverse sets of simulation and experimental studies. In both simulations and experiments, power factor of loads and absolute impedance of critical and non-critical loads are changed to see the changes in the performance of the ES. The system shown in Fig. 1 and specifications listed in Table 1 has been simulated on a MATLAB *Simulink* software platform and experimentally validated on *Infineon* IGBT module with *dSPACE 1104* as the controller. The reference critical

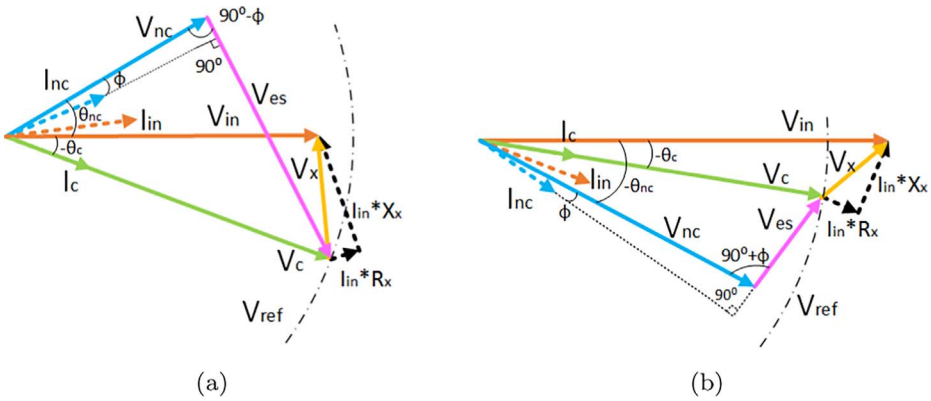

Fig. 6. Phasors of electrical signals in the system with R-L non-critical load (a) in undervoltage scenario ($V_c < V_{ref}$) and (b) in overvoltage scenario ($V_c > V_{ref}$).

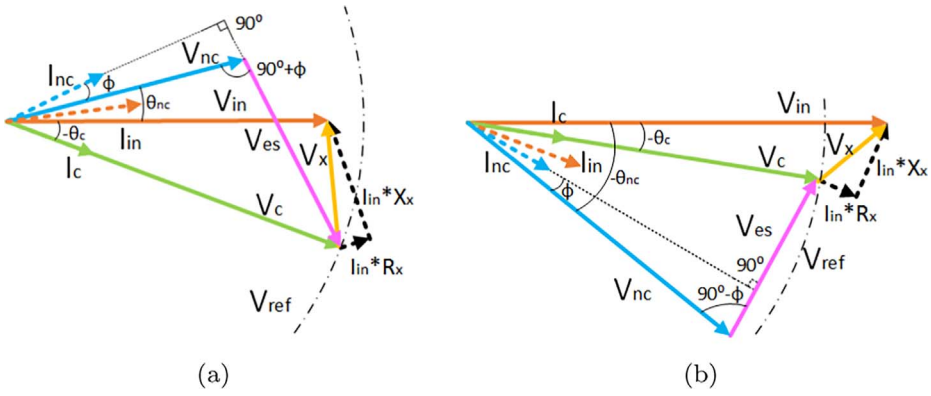

Fig. 7. Phasors of electrical signals in the system with R-C non-critical load (a) in undervoltage scenario ($V_c < V_{ref}$) and (b) in overvoltage scenario ($V_c > V_{ref}$).

Table 1
System specifications.

System parameter	Value
Line impedance	0.1 + j 0.785 Ω
Noncritical load impedance	38 Ω
Critical load impedance	68 Ω
ES power circuit	
Inverter Rating	800 VA
Inverter topology	Single phase H-bridge
Switching frequency	20 kHz
DC bus voltage	200 V
Output low-pass filter	
Inductance	5 mH
Capacitance	10 μF

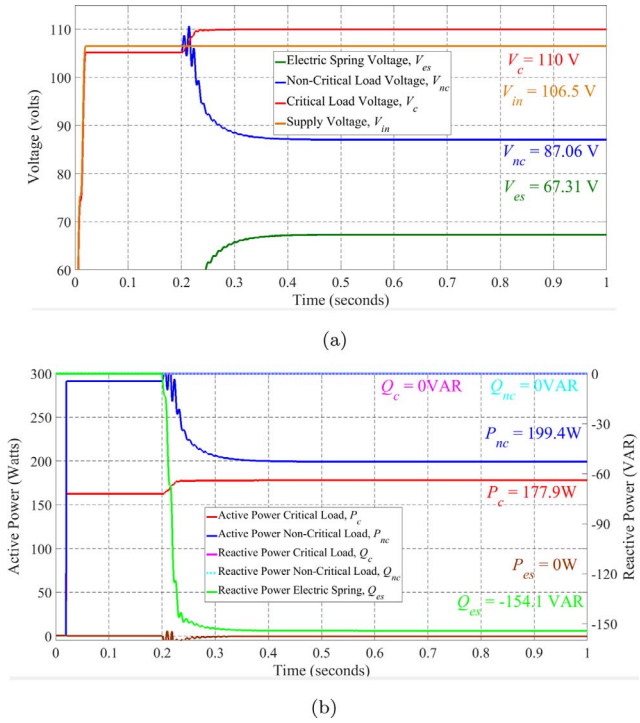

Fig. 8. In undervoltage scenario (ES is turned on at $t = 0.2$ s) (a) RMS voltages, (b) Active and Reactive Power across different components in the system.

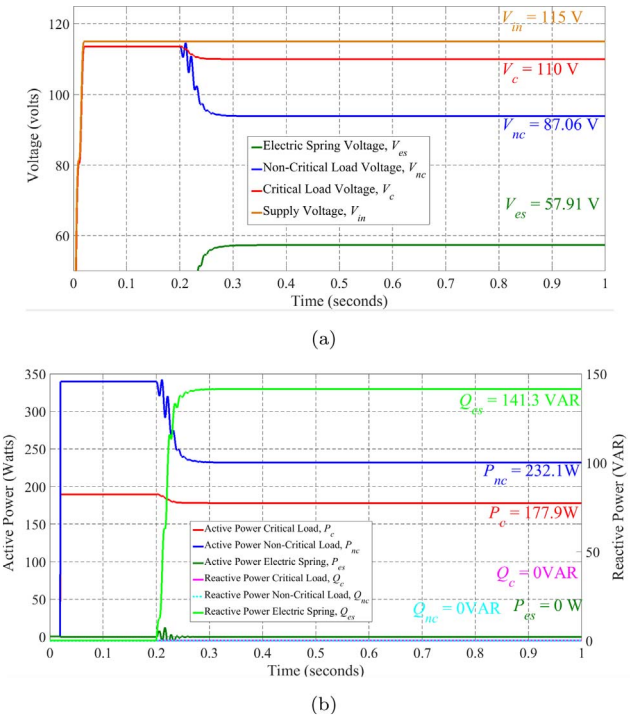

Fig. 9. In overvoltage scenario (ES is turned on at $t = 0.2$ s) (a) RMS voltages, (b) Active and Reactive Power across different components in the system.

load voltage, V_{ref} is set to be 110 V (RMS) at 50 Hz and the line inductance of the system is 2.5 mH.

3.1. Simulation

Through MATLAB *Simulink* software platform, working of the ES is verified in undervoltage and overvoltage scenarios. For a system with resistive non-critical (38 Ω) and critical loads (68 Ω), the voltage and power waveforms are presented. As shown in Fig. 8a, initially (from $t = 0$ s to $t = 0.2$ s), V_c is 105.2 V is less than V_{ref} (110 V). When the ES is turned on at $t = 0.2$ s, V_c increases from 105.2 V to 110 V. In this undervoltage scenario, the ES injects reactive power ($Q_{es} = -154.1$ VAR) as illustrated in Fig. 8b. In overvoltage scenario, when the ES is turned on at $t = 0.2$ s, V_c decreases from 113.6 V to 110 V as depicted in Fig. 9a. In this overvoltage scenario, the ES absorbs reactive power ($Q_{es} = 141.3$ VAR) as shown in Fig. 9b.

Further, rigorous tests by changing the impedance of the critical and non-critical loads and their power factors were performed and various data-sets were recorded. The simulation data were cross-verified with solutions of non-linear mathematical equations of the system. The data

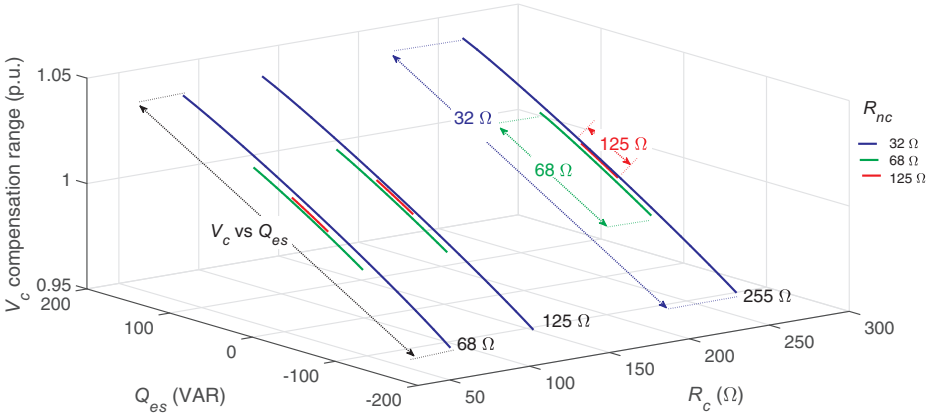

Fig. 10. Performance of ES with change in the critical and non-critical load impedances as observed from simulation data

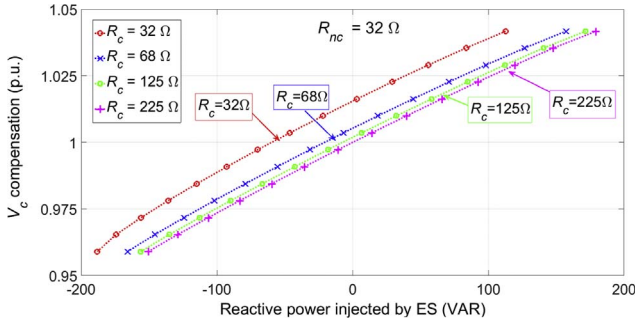

Fig. 11. Performance of ES with change in the critical load's impedance from with constant NC load's impedance as 32 Ω.

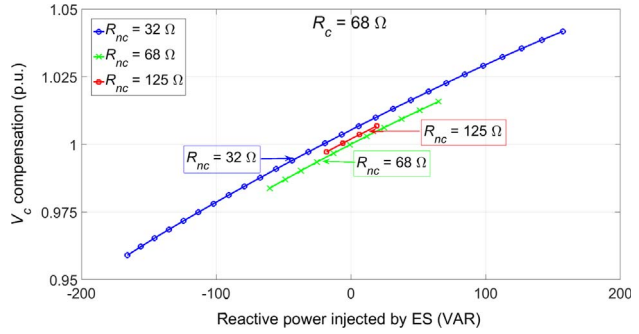

Fig. 12. Performance of ES with change in the noncritical load's impedance from with constant critical load's impedance as 68 Ω.

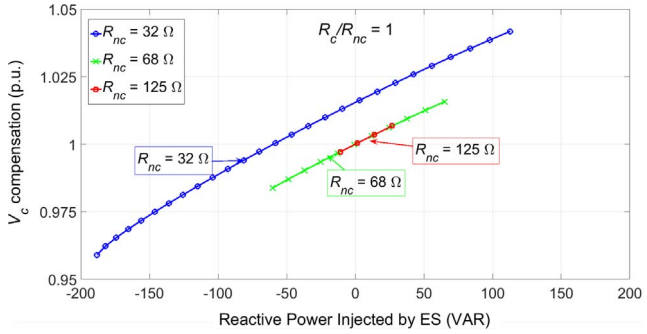

Fig. 13. Experimental observation of compensation range with variation in the non-critical load's impedance with constant ratio of critical and non-critical load impedance; r = 1.

Table 2
Variation in the power factor of Z_c.

Z_c	Z_{nc}
68 Ω	38 Ω
77 + j 68 Ω	38 Ω
68 − j 106 Ω	38 Ω

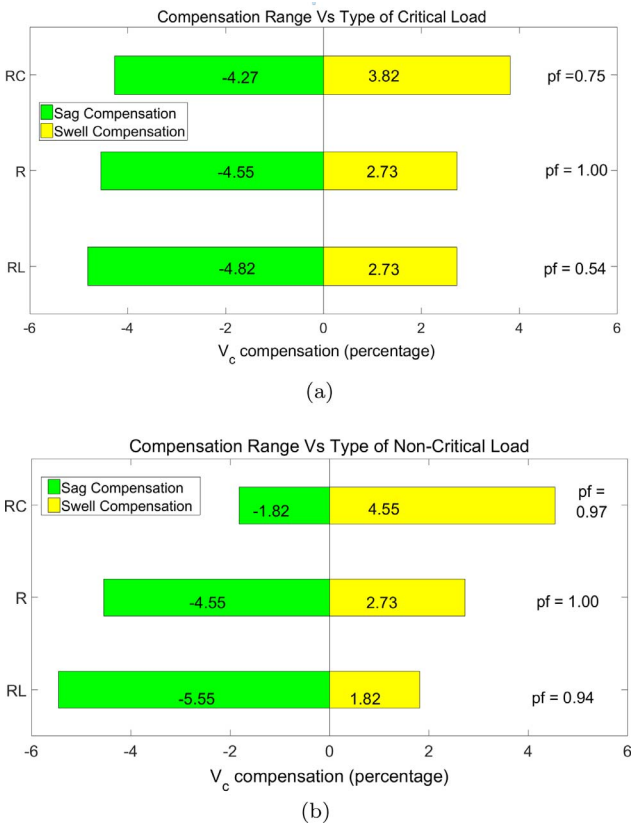

Fig. 14. Performance of the ES with change in the type of the (a) critical load (b) non-critical load.

were analyzed and are presented in a comprehensible way that reflects the performance of the ES under the following conditions:

- change in the critical load impedance,
- change in the non-critical load impedance,
- change in the type of the critical load, and

Table 3
Variation in the power factor of the Z_{nc}.

Z_c	Z_{nc}
68 Ω	38 Ω
68 Ω	$38 + j\ 8.8$ Ω
68 Ω	$38 - j\ 13.3$ Ω

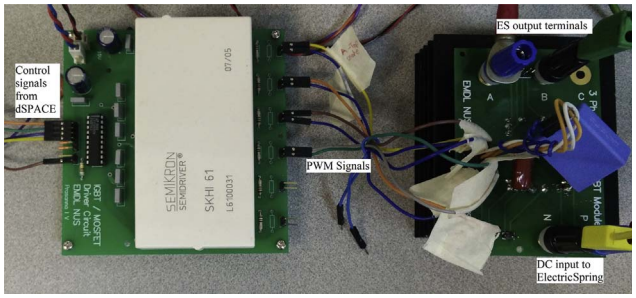

Fig. 15. Infineon IGBT module and Semikron Driver used to implement ES in the hardware setup.

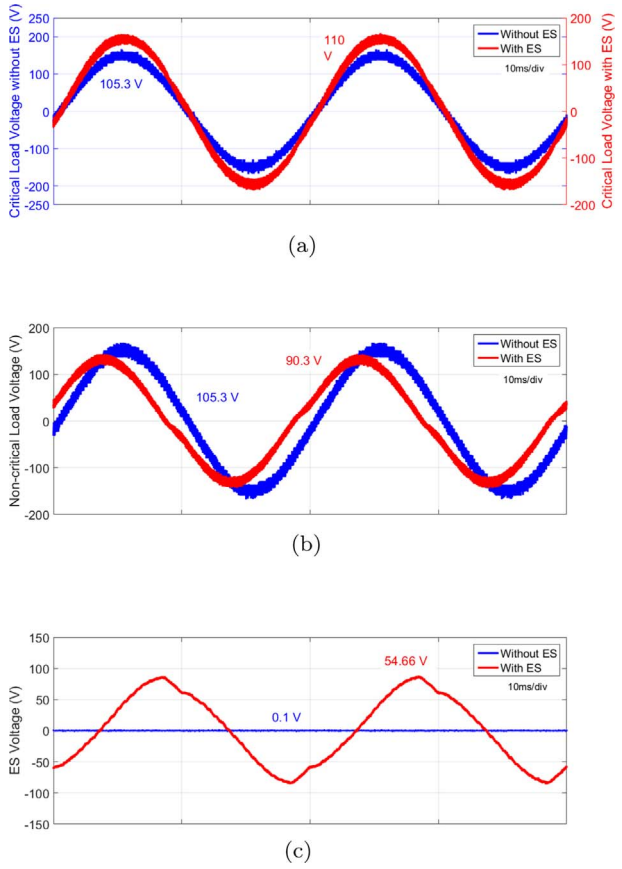

Fig. 16. Voltage waveforms in undervoltage scenario in the experimental system without and with ES for (a) Critical Load Voltage (V_c), (b) Non-critical Load Voltage (V_{nc}), (c) Electric Spring Voltage (V_{es}).

- change in the type of the non-critical load.

3.1.1. Change in the critical load impedance

It is considered that both the NC and critical load are resistive, and R_{nc} (non-critical load resistance) is kept constant and R_c (critical load resistance) is varied and kept at 32 Ω, 68 Ω, 125 Ω, and 255 Ω for three sets of R_{nc} at 32 Ω, 68 Ω, and 125 Ω. As discussed in Section 2.2, behavior of the ES shouldn't change and thus, the compensation range of

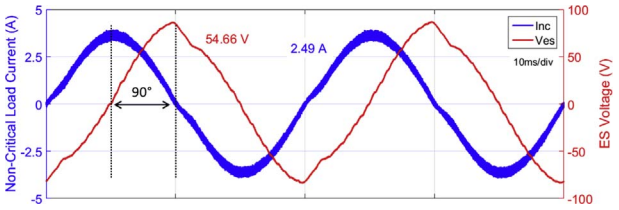

Fig. 17. Non-critical load current (I_{nc}) leads the ES Voltage (V_{es}) by 90°.

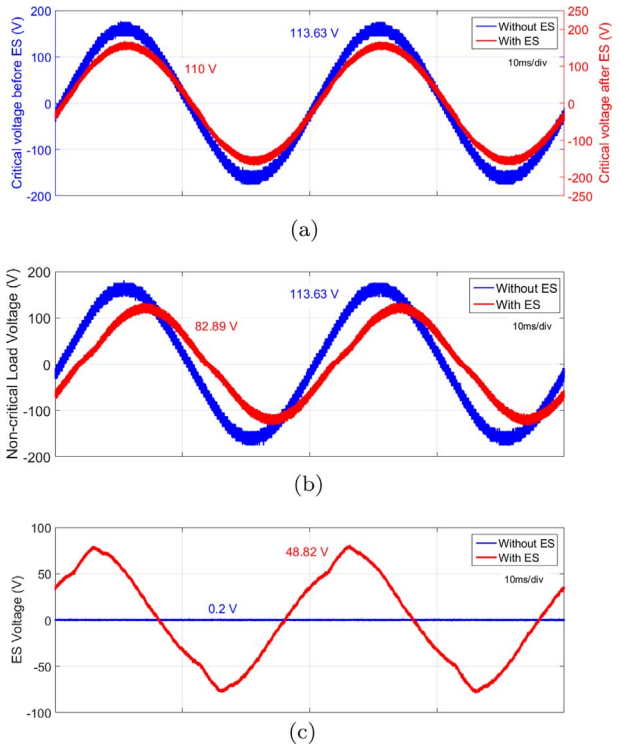

Fig. 18. Voltage waveforms in overvoltage scenario in the experimental system without and with ES for (a) Critical Load Voltage (V_c), (b) Non-critical Load Voltage (V_{nc}), (c) Electric Spring Voltage (V_{es}).

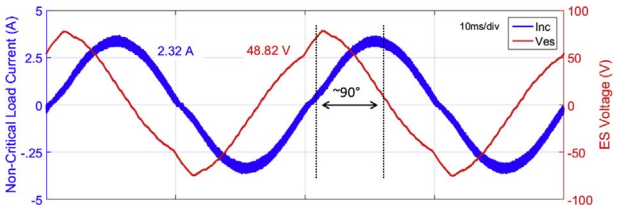

Fig. 19. Non-critical load current (I_{nc}) lags the ES Voltage (V_{es}) by 90°.

critical load voltage (in p.u.) shouldn't change. As seen by Fig. 10, the compensation range remains the same with a constant R_{nc}. Consider the case with $R_{nc} = 32$ Ω (as shown in Fig. 11), the compensation range remains same for different R_c.

3.1.2. Change in the non-critical load impedance

In this case, R_{nc} is varied while maintaining R_c constant, a distinguishable change in the compensation range should be observed. R_{nc} is varied and kept at 32 Ω, 68 Ω, and 125 Ω for three sets of constant R_c at 68 Ω, 125 Ω, and 255 Ω. Fig. 10 illustrates that as R_{nc} decreases, the compensation range of the critical load voltage increases. Consider the case of, $R_c = 68$ Ω (as shown in Fig. 12), the compensation decreases with increase in R_{nc}. Also, the compensation range of the ES depends not just on the ratio of critical load to non-critical load [16], but on the absolute value of non-critical load. It is shown in Fig. 13 for the same

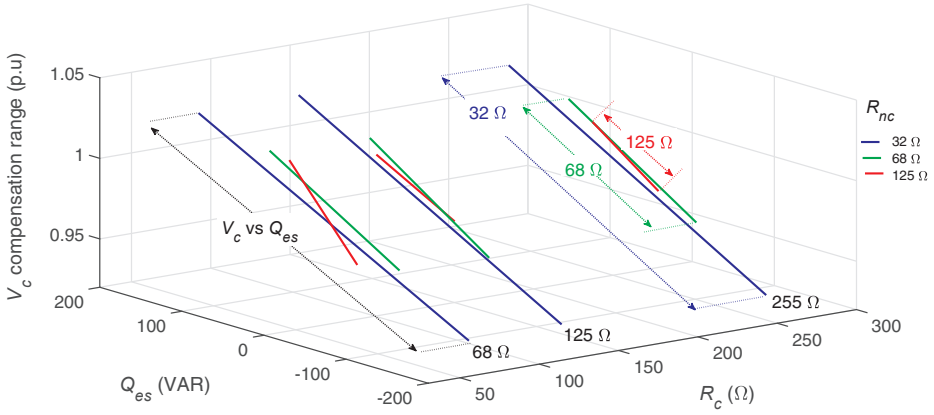

Fig. 20. Performance of ES with change in the critical and non-critical load impedances as observed from experimental data.

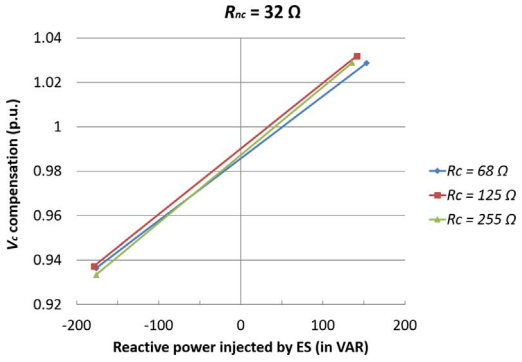

Fig. 21. Experimental observation of compensation range with variation in the critical load's impedance with constant noncritical load impedance as 32 Ω.

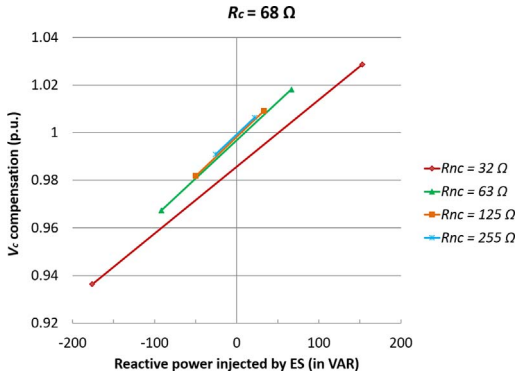

Fig. 22. Experimental observation of compensation range with variation in noncritical load's impedance with constant critical load impedance as 68 Ω.

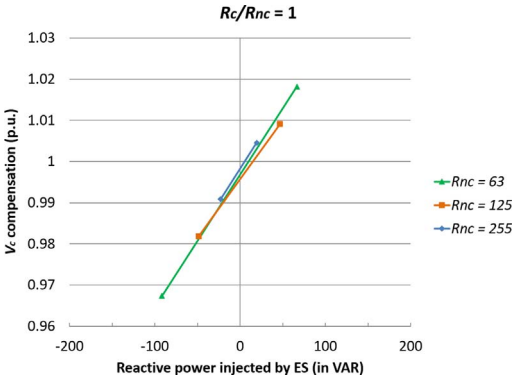

Fig. 23. Experimental observation of compensation range with variation in non-critical load's impedance with constant ratio of critical and non-critical load impedance; r = 1.

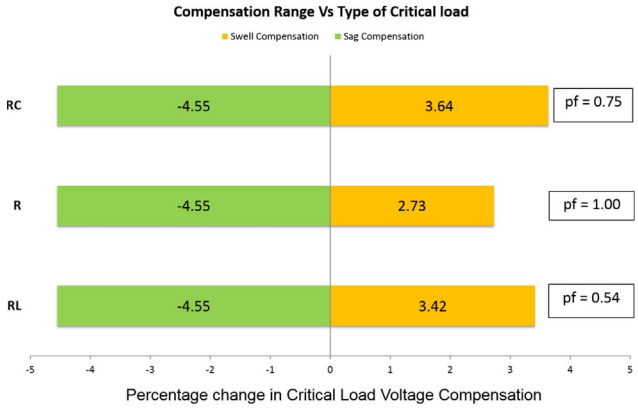

Fig. 24. Experimental observation of compensation range with variation in the critical load's type.

ratio (of critical to non-critical load), the system with the lower non-critical load impedance has a higher compensation range. Due to limitation of space, only one value of ratio is shown, however, the results could be observed for different ratios too. Thus, using this ratio to gauge the performance of the ES would not be enough.

3.1.3. Change in the type of the critical load

The effects of changes in the type of the critical load is studied. While keeping the non-critical load resistive, the type of the critical load is changed to resistive, resistive-inductive, and resistive-capacitive. The values of both the non-critical and the critical load impedances are listed in Table 2. As discussed earlier, the compensation range is dependent on the reactive power compensation by the ES (Q_{es}). However, Q_{es} is not dependent on the critical load impedance and its type. Thus, there should be minimal effect on the compensation range which is confirmed from the simulation results and demonstrated in Fig. 14a.

3.1.4. Change in the type of the non-critical load

The effect of change in the type of the non-critical load is evaluated. While keeping the critical load resistive, the type of the non-critical load is changed from resistive to resistive-inductive and resistive-capacitive. The values of both the non-critical and critical load impedances are listed in Table 3. The impedance of the NC load is maintained constant and at almost the same value. The impedances of RC, R, and RL non-critical load are 39 Ω, 38 Ω, and 40 Ω, respectively. The difference in the impedances isn't significantly large to affect the performance of the ES. This can be corroborated by observing the relationship between non-critical load impedance and performance of the

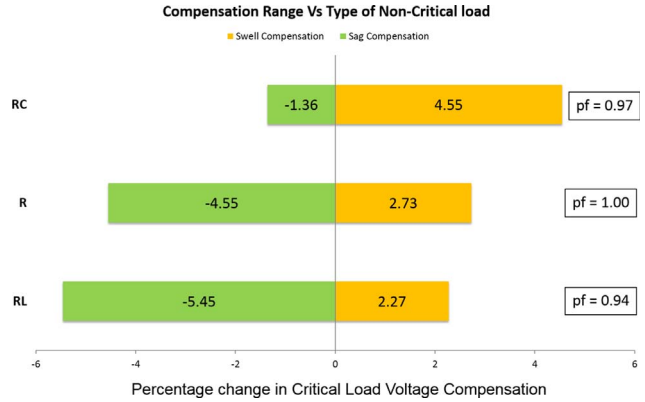

Fig. 25. Experimental observation of compensation range with variation in the non-critical load's type.

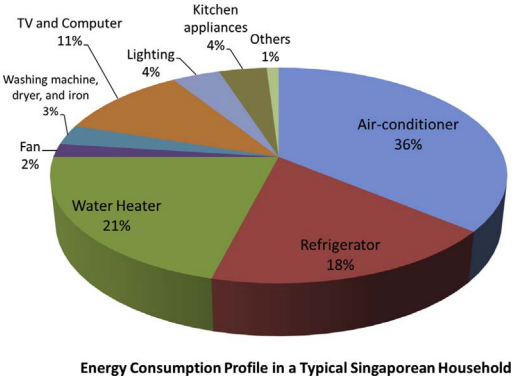

Fig. 26. Distribution of electricity consumption in a typical Singaporean household [28].

ES as shown in Fig. 12.

It has been discussed in Section 2.3 that due to the limitations on the amount of reactive power in the system, the compensation range would change with changes in the types of the non-critical load. As illustrated in Fig. 14b, with a R-L NC load we see an increase in boosting range and a decrease in reduction range (with respect to a resistive NC load). Conversely, with a R-C NC load, a decrease in boosting range and an increase in reduction range is observed (with respect to a resistive NC load). This verifies the claims.

3.2. Experiment

The Electric Spring was implemented using an *Infineon* IGBT module FS25R-12W1T4 and *Semikron* IGBT driver SKHI 61 shown in Fig. 15 and was controlled using *dSPACE 1104*. Similar to the simulation studies, the experiments were performed to validate the working of the ES and to evaluate the performance of the ES subjected to the same conditions as outlined in Section 3.1.

The working of the ES was verified in undervoltage and overvoltage scenarios. For a system with resistive non-critical (38 Ω) and critical loads (68 Ω), the voltage and current waveforms are presented. In the undervoltage scenario, the input voltage (V_{in}) for the system without and with the ES remains same at 108.19 V. The steady-state waveforms of the voltage signals without and with ES are illustrated in Fig. 16. The ES is able to boost V_c from 105.3 V to 110 V. The non-critical load voltage, V_{nc} decreases from 105.3 V to 90.3 V, and V_{es} increases from 0 V to 54.66 V. It can be seen that I_{nc} leads V_{es} by 90° (Fig. 17) thus indicating that the ES injects only reactive power in the system or the ES acts as a capacitor.

Similarly, in the overvoltage scenario, V_{in} without and with the ES remains same at 116.29 V. The steady-state waveforms of the voltage signals are shown in Fig. 18. The ES is able to reduce V_c from 113.63 V to 110 V, V_{nc} decreases from 113.63 V to 82.89 V, and V_{es} increases from 0 V to 48.82 V. It can be seen that I_{nc} lags V_{es} by 90° (Fig. 19) thus indicating that the ES absorbs only reactive power in the system or the ES acts as an inductor.

The waveform of the ES voltage is distorted and not purely sinusoidal due to the dead time provided between switches of the same legs in voltage source converter to prevent shoot through the switches. During the dead time, both switching devices are off, and one of the two anti-parallel diodes of the switching devices conduct according to the polarity of the pole current which introduces a positive or negative error in the ES voltage. Because of this error, the magnitude of the fundamental output voltage deviates from its reference, and lower order harmonics are introduced in the output voltage. This effect is amplified in a grid-connected system, such as one present here, because the output filter is designed to attenuate only the high-frequency switching ripple. The slight phase difference between the ES voltage and the non-critical load current is due to the losses incurred in the inverter. This can be corrected by calculating the losses in the inverter and adding the resultant phase shift to maintain 90° phase shift between the ES voltage and the non-critical load current.

3.2.1. Change in the critical load impedance

In this case, resistive critical and non-critical loads are considered and R_c is varied while maintaining R_{nc} constant. This experiment is performed by varying R_c to 68 Ω, 125 Ω, and 255 Ω for the following sets of R_{nc} 32 Ω, 63 Ω, and 125 Ω. The performance of the ES is recorded and analyzed and depicted in Fig. 20. Similar to the simulations, the compensation range of the critical load voltage doesn't change much with the change in the impedance of critical load. This validates the claim in Section 2.2 that the compensation range is not dependent the critical load impedance (see Fig. 21).

3.2.2. Change in the non-critical load impedance

Further, to test the effect of the non-critical load impedance on the performance of the ES, it is varied while maintaining the critical load impedance constant. This experiment is performed by varying R_{nc} to 32 Ω, 63 Ω, and 125 Ω for the following sets of R_c 68 Ω, 125 Ω, and 255 Ω. The performance of the ES is recorded and analyzed and depicted in Fig. 20. The compensation range of the critical load voltage increases as the NC load impedance decreases, thus validating the claim in Section 2.2 (see Fig. 22).

Another point to be noted is that the compensation range of the critical load voltages, doesn't vary just with the ratio of critical and non-critical loads, but does with the absolute value of the non-critical load. This is highlighted in Fig. 23 where for each ratio of critical and non-critical load is kept same and non-critical impedance is varied. It is observed that despite the same ratio of critical and non-critical loads, compensation range increases as the impedance of NC load decreases.

3.2.3. Change in the type of the critical load

For analyzing the effects of type of critical load on performance of the ES, impedance of the critical load is changed (Table 2). The non-critical load is kept resistive and the type of the critical load is changed to resistive, resistive-inductive, and resistive-capacitive. Similar to simulations, it is observed that change in type of critical load minimally affect the compensation range (Fig. 24). The reason for this is that the reactive power compensation (Q_{es}) is not dependent on critical load's impedance and its type as highlighted in Section 2.3.

3.2.4. Change in the type of the non-critical load

The impedance of non-critical load is changed (Table 3) to analyze the effect of the type of the NC load on compensation range. The critical load is kept resistive and the type of the non-critical load is changed to resistive, resistive-inductive, and resistive-capacitive. When the R-L non-critical load was used the boosting range increased and the reduction range decreased (compared to the resistive NC load). While

with the R-C non-critical load the boosting range decreased and the reduction range increased (compared to the resistive NC load). The effects in change of NC load's type are reflected in Fig. 25. These are in line with the claims presented in Section 2.3, which state that the compensation range changes so as to not to violate the reactive power limits of the system.

Through simulation and experimental studies, it has been observed that the ES, irrespective of the load type, injects reactive power to boost the critical load voltage and absorbs reactive power to reduce the critical load voltage. It has also been concluded that the performance of the ES is not affected by the critical load impedance and its type. However, the performance of the ES is significantly dependent upon the type and the impedance of the non-critical load. The compensation range provided by the ES increases with decrease in noncritical load impedance.

4. Remarks on selection of non-critical loads

It has been established, through simulations and experimental validation, that selection of non-critical load would play a crucial role in determining the performance of the Electric Spring. The ES can provide a wider range of compensation if there's more non-critical load in the system. The distribution of household electricity consumption is given by Fig. 26. The loads like air-conditioning, refrigerator, water heater, and fan could be classified as non-critical loads [6] which would account for 77% of the household electricity consumption [28]. Also, in a tropical area loads like air-conditioning and fans are fixed and perennial in nature; thus desired characteristics from the ES could be obtained. It is our recommendation to have one ES per household and typically in series with loads embedded in fixture like water heaters, air-conditioners, fans, etc. and not plug-in loads like washing machines and dryer. This would mean the system might need to be retrofitted, however a long term energy reduction and cost savings should justify the necessary retrofitting cost.

5. Conclusions and discussion

Electric Spring, a fledgling technology, is employed to maintain voltage and power stability in an isolated microgrid system with voltage variation from a RES in two scenarios namely undervoltage and overvoltage. The feasibility and operating principles of the reactive power compensating ES is demonstrated and validated through simulations and experiments with linear loads. The ES injects reactive power in the system to boost the critical load voltage and absorbs reactive power to reduce the critical load voltage irrespective of the change in load types of either critical or non-critical loads.

Further, the performance of the ES is gauged on the variation of both the critical and non-critical load impedances and their load types. It is found that the absolute impedance and type of the critical load doesn't affect the performance of the ES. However, as we vary non-critical impedances and types, significant impact on the performance of the ES is observed. As the non-critical load impedance is reduced, the compensation range of critical load voltage improves. The performance of the ES is affected by the type of non-critical load. With RL non-critical load, the boosting range increases whereas with RC non-critical load it decreases. And, reduction range decreases with RL non-critical load and increases with RC non-critical load.

This paper has introduced key concepts and filled the gaps in literature on the ES with only reactive power compensation. It has also highlighted how the performance of the ES relies heavily on the system configuration, which would help devise future control mechanisms. The performance analysis of the ES using motor loads and nonlinear loads is currently under research and would be presented in future work. The learnings from this paper could be utilized for a comparative analysis of performance of various versions of the ES.

Acknowledgment

This research is funded by the Republic of Singapore's National Research Foundation through a grant (R-263-000-A34-592) to the Berkeley Education Alliance for Research in Singapore (BEARS) for the Singapore-Berkeley Building Efficiency and Sustainability in the Tropics (SinBerBEST) Program. BEARS has been established by the University of California, Berkeley as a center for intellectual excellence in research and education in Singapore.

References

[1] Olivares DE, Mehrizi-Sani A, Etemadi AH, Cañizares CA, Iravani R, Kazerani M, et al. Trends in microgrid control. IEEE Trans Smart Grid 2014;5(4):1905–19. http://dx.doi.org/10.1109/TSG.2013.2295514.
[2] Puttgen HB, MacGregor PR, Lambert FC. Distributed generation: Semantic hype or the dawn of a new era? IEEE Power Energ Mag 2003;1(1):22–9.
[3] Singapore energy statistics 2015; Jun 2015. URL <https://www.ema.gov.sg/cmsmedia/Publications_and_Statistics/Publications/ses/2015/index.html>.
[4] Enslin JH. Power system infrastructure: Do we face a complete power-electronics-based power system and energy-storage infrastructure? IEEE Power Electron Mag 2016;3(2):42–5. http://dx.doi.org/10.1109/MPEL.2016.2551798.
[5] Zibelmen A. Reving up the energy vision in New York: Seizing the opportunity to create a cleaner, more resilient, and affordable energy system. IEEE Power Energ Mag 2016;14(3):18–24. http://dx.doi.org/10.1109/MPE.2016.2524967.
[6] Hui SY, Lee CK, Wu FF. Electric springs – a new smart grid technology. IEEE Trans Smart Grid 2012;3(3):1552–61. http://dx.doi.org/10.1109/TSG.2012.2200701.
[7] Hui S, Lee C, WU F. Power control circuit and method for stabilizing a power supply; 2012. URL <http://www.google.com/patents/US20120080420>.
[8] Tan SC, Lee CK, Hui SY. General steady-state analysis and control principle of electric springs with active and reactive power compensations. IEEE Trans Power Electron 2013;28(8):3958–69. http://dx.doi.org/10.1109/TPEL.2012.2227823.
[9] Lee CK, Chaudhuri B, Hui SY. Hardware and control implementation of electric springs for stabilizing future smart grid with intermittent renewable energy sources. IEEE J Emerging Sel Top Power Electron 2013;1(1):18–27. http://dx.doi.org/10.1109/JESTPE.2013.2264091.
[10] Soni J, Krishnanand KR, Panda SK. Load-side demand management in buildings using controlled electric springs. In: IECON 2014 – 40th Annual conference of the IEEE industrial electronics society; 2014. p. 5376–81. http://dx.doi.org/10.1109/IECON.2014.7049321.
[11] Lee CK, Hui SY. Reduction of energy storage requirements in future smart grid using electric springs. IEEE Trans Smart Grid 2013;4(3):1282–8. http://dx.doi.org/10.1109/TSG.2013.2252208.
[12] Soni J, Panda SK. Electric spring for voltage and power stability and power factor correction. IEEE Trans Ind Appl 2017;53(4):3871–9. http://dx.doi.org/10.1109/TIA.2017.2681971.
[13] Mok KT, Tan SC, Hui SYR. Decoupled power angle and voltage control of electric springs. IEEE TransPower Electron 2016;31(2):1216–29. http://dx.doi.org/10.1109/TPEL.2015.2424153.
[14] Wang Q, Cheng M, Chen Z. Steady-state analysis of electric springs with a novel delta control. IEEE Trans Power Electron 2015;30(12):7159–69. http://dx.doi.org/10.1109/TPEL.2015.2391278.
[15] Shuo Y, Tan SC, Lee CK, Hui SYR. Electric spring for power quality improvement. In: 2014 IEEE applied power electronics conference and exposition – APEC 2014; 2014. p. 2140–47. http://dx.doi.org/10.1109/APEC.2014.6803602.
[16] Chaudhuri NR, Lee CK, Chaudhuri B, Hui SYR. Dynamic modeling of electric springs. IEEE Trans Smart Grid 2014;5(5):2450–8. http://dx.doi.org/10.1109/TSG.2014.2319858.
[17] Yang Y, Ho SS, Tan SC, Hui SYR. Small-signal model and stability of electric springs in power grids. IEEE Trans Smart Grid PP 2016(99):1. http://dx.doi.org/10.1109/TSG.2016.2569618.
[18] Akhtar Z, Chaudhuri B, Hui SYR. Primary frequency control contribution from smart loads using reactive compensation. IEEE Trans Smart Grid 2015;6(5):2356–65. http://dx.doi.org/10.1109/TSG.2015.2402637.
[19] Chen X, Hou Y, Tan SC, Lee CK, Hui SYR. Mitigating voltage and frequency fluctuation in microgrids using electric springs. IEEE Trans Smart Grid 2015;6(2):508–15. http://dx.doi.org/10.1109/TSG.2014.2374231.
[20] Yan S, Lee CK, Yang T, Mok KT, Tan SC, Chaudhuri B, et al. Extending the operating range of electric spring using back-to-back converter: Hardware implementation and control. IEEE Trans Power Electron 2017;32(7):5171–9. http://dx.doi.org/10.1109/TPEL.2016.2606128.
[21] Mok KT, Wang MH, Tan SC, Hui SY. Dc electric springs – an emerging technology for dc grids. In: 2015 IEEE applied power electronics conference and exposition (APEC); 2015. p. 684–90. http://dx.doi.org/10.1109/APEC.2015.7104424.
[22] Wang Q, Cheng M, Jiang Y, Chen Z, Deng F, Wang Z. Dc electric springs with dc/dc converters. In: 2016 IEEE 8th international power electronics and motion control conference (IPEMC-ECCE Asia); 2016. p. 3268–73. http://dx.doi.org/10.1109/IPEMC.2016.7512818.
[23] Yang Y, Tan Sc, Hui SYR. Mitigating distribution power loss of dc microgrids with dc electric springs. IEEE Trans Smart Grid PP 2017(99):1. http://dx.doi.org/10.1109/TSG.2017.2698578.
[24] Lee CK, Cheng KL, Ng WM. Load characterisation of electric spring. In: 2013 IEEE

energy conversion congress and exposition; 2013. p. 4665–70. http://dx.doi.org/10.1109/ECCE.2013.6647326.
[25] Lee CK, Chaudhuri NR, Chaudhuri B, Hui SYR. Droop control of distributed electric springs for stabilizing future power grid. IEEE Trans Smart Grid 2013;4(3):1558–66. http://dx.doi.org/10.1109/TSG.2013.2258949.
[26] Kundur P, Balu N, Lauby M. Power system stability and control, discussion paper series. McGraw-Hill; 1994. URL <https://books.google.com.sg/books?id=2cbvyf8Ly4AC>.
[27] Majumder R. Some aspects of stability in microgrids. IEEE Trans Power Syst 2013;28(3):3243–52. http://dx.doi.org/10.1109/TPWRS.2012.2234146.
[28] Singapore's climate action plan: Take action today, for a carbon-efficient singapore, National Climate Change Secretariat Prime Minister's Office Singapore; 2016. URL <https://www.nccs.gov.sg/sites/nccs/files/NCCS_Mitigation_FA_webview%2027-06-16.pdf>.